OPEN ACCESS

Electrochemical/Photoelectrochemical Water Splitting on Self-Limiting Electrodeposited Iron-Group Mutual Alloys

To cite this article: Yin Xu *et al* 2023 *J. Electrochem. Soc.* **170** 056511

Journal of The Electrochemical Society, 2023 **170** 056511

Electrochemical/Photoelectrochemical Water Splitting on Self-Limiting Electrodeposited Iron-Group Mutual Alloys

Yin Xu,[1] Qiyuan Lin,[1] Yunkai Sun,[1] Rasin Ahmed,[1] Massimo Innocenti,[2,3,4] and Giovanni Zangari[1,z]

[1]*Department of Materials Science and Engineering, University of Virginia, Charlottesville,Virginia 22904, United States of America*
[2]*National Interuniversity Consortium of Materials Science and Technology (INSTM), 50121 Firenze (FI), Italy*
[3]*Center for Colloid and Surface Science (CSGI), 50019 Sesto F.no (FI), Italy*
[4]*Institute of Chemistry of Organometallic Compounds (ICCOM)—National Research Council (CNR), 50019 Sesto Fiorentino, Italy*

Scalable energy conversion/storage by water splitting is significantly hindered by the slow kinetics of oxygen evolution reaction (OER). Implementation of electrochemical catalysts with low cost and high turn-over efficiency, or application of a photoanode in photoelectrochemical (PEC) cell using a semiconductor with proper protection layer are two possible solutions. Herein, two binary Iron-group alloy films (Ni-Co and Ni-Fe) and one ternary Iron-group alloy film (Ni-Co-Fe) under self-limiting deposition condition are investigated and continuous ultrathin films with various composition are generated. The self-limiting deposition, corroborated by XPS depth profile, is caused by the precipitation of hydroxide/oxyhydroxide species under high local pH, enabled by the privation of pH buffer species. Each binary and ternary Iron-group mutual alloy films exhibits improved water oxidation kinetics compared to pure i or Co film. In particular, an overpotential of 0.314 V at 10 mA cm^{-2} and a Tafel slope of 34.7 mV dec^{-1} are obtained on the Ni-Fe-Co film. The Iron-group mutual alloy deposited GaAs is further investigated for photoelectrochemical water oxidation. The stability towards photocorrosion under the light in an aqueous solution containing $K_3Fe(CN)_6/K_4Fe(CN)_6$ is significantly improved by electrodepositing the mutual alloy films while the optimum stability property is found on the ternary alloy film.

 [DOI: 10.1149/1945-7111/acd663]

Manuscript submitted December 16, 2022; revised manuscript received March 24, 2023. Published May 30, 2023.

Low-cost and high-purity hydrogen generation can be rationalized by splitting water into hydrogen and oxygen using electrical or solar energy.[1–4] The slow kinetics of oxygen evolution reaction (OER), however, is an essential limitation due to the four electron transfer process and the formation of oxygen-oxygen bond.[5] Electrocatalysis or photo-electrocatalysis are among the most promising approaches in overcoming this limitation of OER.[6] In particular, Earth abundant electrochemical catalysts with high catalytic activity and stability are usually required in order to exceed the large activation barriers and minimize the input electrical energy; semiconductors with appropriate protective catalyst layer in a photoelectrochemical (PEC) device allows significant OER overpotential reduction owed to the oxidation introduced by photo-generated holes.[7] In either scenario, inexpensive and simple method to deposit thin-film catalysts with high turn-over efficiency, complete coalescence and versatile in composition-control is particularly in demand.

Various configurations are available to generate photovoltage and extract the holes from the semiconductor. In this work we fabricate a metal-insulator-semiconductor (MIS) in contact with a Schottky junction. The GaAs was used as the semiconductor for the photoanode. To avoid photocorrosion, the GaAs is protected by one or several monoatomic layer of Iron-group metal on a flat substrate synthesized by the self-limiting electrodeposition.[8]

The self-limiting growth of iron group metals (Co, Fe, Ni) is generated by limiting (and in some cases fully removing) buffers, such as boric acid (H_3BO_3): the privation of a boric buffer induces over time an increase of local pH due to excess OH^- species generated from the hydrogen evolution reaction at the cathode, resulting in precipitation of a compact hydroxide/oxyhydroxide layer on the surface. The compact hydroxide/oxyhydroxide layer, due to low conductivity, can further terminate growth, leading to the formation of a continuous ultrathin (oxy) hydroxide/metal film.

The mechanism was developed and understood by Vanpaemel, Veerecken et al. They reported purposely electrodeposition of ultrathin Ni layer on top of TiN substrate by evaluating the effect of buffer species. Films were then applied as the catalyst for carbon nanotube growth.[9,10] Moffat et al. used Au ultramicroelectrodes to study the self-limiting electrodeposition of Ni and Ni hydroxide formation,[11] and extended the self-limiting deposition to Fe and Co in a potentiostatic condition.[12] Up to now, no systematic study can be found on the self-limiting electrodeposition of binary alloy films, let alone ternary alloy system. In addition, no efforts on the electrochemical /photoelectrochemical property of the Iron-group metal/alloys have been reported so far.

In this work, we use galvanostatic electrodeposition for synthesizing two binary Iron-group mutual alloy films (Ni-Co, and Ni-Fe) and a ternary Iron-group mutual alloy film in a self-limiting deposition condition. The self-limiting deposition mechanism is proved by potential transient, XPS spectrum and XPS depth profile, from which an independence of the film thickness towards deposition time is demonstrated. Adding an additional element during deposition is proven to introduce a slower nucleation as a result of the smaller grain size of the deposited nanoislands. The electrochemical catalytic activity of the Iron-group alloy films was investigated and the water oxidation on the trinary film exhibits significantly improved kinetics. Furthermore, the Iron-group mutual alloy films were deposited on GaAs, which showed enhanced stability in photoelectrochemical water oxidation while retained a high photoresponse simultaneously.

Experimental

Electrodeposition of mutual Iron-group alloys.—Chemicals used in this work were all purchased from Sigma Aldrich (analytical grade) without further purification. For all the deposition, a three-electrode system was applied with Pt mesh as the counter electrode, saturated calomel electrode (SCE) as the reference electrode, and Au/Si (Polycrystalline (111) textured on Si wafer) or GaAs (Si doped, 0.8–4 × 10^{18} cm^{-3}, (100) orientation) substrate as the

[z]E-mail: gz3e@virginia.edu

working electrode. Au substrates were immersed in 0.5 s H_2SO_4 for 30 s, rinsed with DI water and dried by air gun to remove impurities and oxides on the surface before deposition. GaAs substrates were rinsed with acetone for 2 min, 10% ammonia for 2 min. and DI water for 30 s sequentially to remove the surface oxides, and then an Ohmic contact between the substrate and current collector was made by liquid eutectic GaIn prior to electrodeposition.[13] Pure Ni film was electrodeposited in a solution containing 15 mM $NiCl_2{\cdot}6H_2O$ and 100 mM KCl;[10] pure Co film was prepared using a solution containing 15 mM $CoCl_2{\cdot}6H_2O$ and 100 mM KCl; Ni-Co film was deposited in a solution containing $NiCl_2{\cdot}6H_2O$, $CoCl_2{\cdot}6H_2O$ (total concentration is 20 mM) and 100 mM KCl; Ni-Fe film was prepared in a solution containing $NiCl_2{\cdot}6H_2O$, $FeCl_2{\cdot}4H_2O$ (total concentration is 20 mM) and 100 mM KCl with N_2 purging for 0.5 h prior to the deposition. Ni-Fe-Co film was prepared in a solution containing 15 mM $NiCl_2{\cdot}6H_2O$, 5 mM $FeCl_2{\cdot}4H_2O$, 5 mM $CoCl_2{\cdot}6H_2O$ and 100 mM KCl. The solution pH was adjusted to 3.0 by 1 M HCl. All the films were deposited at a constant current density of 10 mA cm^{-2} with the deposition time ranging from 0.2 s to 60 s (EG&G PAR Model 273 A potentiostat).

Characterization.—Chemical state changes and elemental composition on the surface and along the out-of-plane depth were measured using an X-ray photoelectron spectroscopy (XPS, PHI 5000 VersaProbe III, Al Kα) coupled with an Ar^+ ion sputtering gun. The comparison of the grain sizes of Ni and Ni-Fe was estimated using grazing incidence X-ray diffraction (GI-XRD, PANalytical Empyrean X-ray diffractometer, Cu Kα, $\lambda = 1.54$ Å). The surface morphology and bulk composition were investigated using a field emission scanning microscope (FE-SEM, FEI Quanta 650 SEM) coupled with an energy dispersive X-ray spectroscopy (EDS).

Electrochemical/Photoelectrochemical measurements.—Electrochemical water oxidation property was measured using a three-electrode system with Pt mesh as the counter electrode, SCE as the reference electrode and the deposited metal/alloys on Au substrate as the working electrode in 1 M KOH solution (pH = 13.6) at room temperature. Cyclic voltammetries and linear scanning voltammetries were performed in a potential range from −0.2 V to 1.0 V vs SCE at a scanning rate of 10 mV s^{-1}. Tafel plots were measured by recording the steady state potential at a series of constant current density. The IR potential drop was compensated by measuring the solution resistance using EIS method before the electrochemical water oxidation tests. Photo-water oxidation performance was evaluated in a high-concentration aqueous Ferricyanide/Ferrocyanide solution (50 mM $K_3Fe(CN)_6$, 350 mM $K_4Fe(CN)_6$ and 1 M Na_2SO_4; pH = 6.7) with Pt mesh as the counter electrode, SCE as the reference electrode and the deposited metal/alloys on GaAs substrate as the working electrode under AM 1.5 G solar irradiation (100 mW cm^2; Oriel Sol 1 A solar simulator). Linear scanning voltammetries were measured at a scanning rate of 10 mV s^{-1} from −0.8 V to 1.2 V vs SCE under chopped light. The stability towards photocorrosion was evaluated at a constant potential of 1.23 V vs RHE under illumination. All the potentials shown in this work were converted to the reversible hydrogen electrode reference (RHE) using the Nernst equation ($E^o_{RHE} = E_{app} + 0.059 \times pH + E^o_{SCE}$).

Results and Discussion

Electrodeposition of iron-group binary alloys.—Potential transients of Ni and CoNi deposition in the first second is shown in Fig. 1a. Typically, the potential transients is an indicator of the nucleation and first stage of growth. For either deposition, a rapid increase in the potential occurs in the first ∼0.2 s corresponding to the charging of the electrode and the formation of electrochemical double layer before the nucleation initiates. A bump in the potential appears at 0.4 s to 0.6 s for Ni deposition while a similar bump for Ni-Co deposition appears at 0.6 to 0.8 s, which indicates the formation of hydroxide/oxyhydroxide layer induced by the local pH gradient without buffer species.[9] A second bump is shown at ∼0.8 s for Ni and at ∼1.0 s for Ni-Co deposition, corresponding to the completion of the surface hydroxide/oxyhydroxide formation. This surface layer is usually compact and is able to terminate further growth, resulting in an ultrathin metal/ (oxy) hydroxide layer with full coalescence, which is a significant feature of the self-limiting deposition.[10] The current density is mainly contributed by intense hydrogen evolution after the continuous surface layer is formed, as bubble formation was observed after ∼1 s of deposition. It needs to be noted the Ni-Co deposition has a delayed nucleation (∼0.2 s) at both initial state (first bump in potential transient curve) and the completion of the nucleation (second bump) compared to pure Ni deposition, as more nucleation sites with smaller sizes are formed by adding Co. The chemical state changes of the as-deposited Ni-Co film on Au were further investigated by XPS. The XPS spectrum of the Ni-Co film without/with a 6 s Ar milling (∼removal of 1.5 nm surface layer) is compared as shown in Figs. 1b–1d. The peak located at a binding energy of 854.6 eV for the pre-sputtered Ni-Co film is assigned to the Ni $2p_{3/2}$ in NiO, indicating that the surface Ni mainly exists in the form of NiO. A metallic Ni peak with a binding energy of 853.0 eV appears after sputtering while a shoulder peak at 856.2 eV next to the NiO peak is associated with NiOOH as shown in Fig. 1b. For Co spectrum, a broad peak with its maximum intensity located at 780.4 eV is shown for both of the pre-sputtered and post-sputtered Ni-Co film in Fig. 1c, which is corresponding to Co $2p_3/_2$ in the form of Co_2O_3 or Co_3O_4. The broad peak probably consists of multiple peaks from other Co oxides, hydroxides, or oxyhydroxides, which is however difficult to specify. The oxygen peak located at 530.0 eV before Ar sputtering is associated with the O-H bond from absorbed water or surface hydroxides/oxyhydroxides, while the intensity of this peak decreases after sputtering and another peak located at 532.0 eV corresponding to Ni^{3+} or Co^{3+} is present. This result is in good agreement with the Ni 2p and Co 2p spectrum.

Potential transient of Ni-Fe deposition is shown in Fig. 2a. Similar to the case of Ni-Co, the first bump occurs at ∼0.6−0.8 s while the second bump is not found in the first second of deposition, which indicates a similar self-liming growth and an even slower nucleation process for Ni-Fe deposition compared to pure Ni deposition and Ni-Co deposition. XPS spectrums of the Ni-Fe deposited film are shown in Figs. 2b–2d without/with 6 s Ar sputtering. Prior to sputtering, the peaks occurring at a binding energy of 852.6 eV is assigned to metallic Ni while the one located at 855.6 eV can be assigned to NiOOH as shown in Fig. 2b. The NiOOH peak disappears while the intensity of metallic Ni peak increases after Ar sputtering, showing Ni in the film underneath the surface mainly exists in the form of metallic Ni. For Fe spectrum shown in Fig. 2c, a broad peak with the maximum intensity located at 712.2 eV is associated with FeOOH, while multiple overlapped peaks from other Fe oxides/hydroxides possibly contribute to the main peak as well.

In order to further demonstrate the self-limiting mechanism for Ni-Co and Ni-Fe deposition, elemental composition measured by XPS along the out-of-plane depth of the film vs different Ar milling depth was investigated for the films deposited with different time. As shown in Fig. 3a, for both the 10 s deposited and 60 s deposited Ni-Co, Ni and Co deposition starts to decrease with a corresponding increase of Au composition after the first Ar sputtering, indicating that interdiffusion occurs among Ni, Co and Au substrate. When the milling depth reaches ∼17 nm, the composition of Au becomes ∼100% and stays constant while all the other elements cannot be detected, such that a layer thickness of ∼17 nm of the surface plus the interdiffusion layer is determined for both 10 s deposited and 60 s deposited Ni-Co. The independence of layer thickness on different deposition time further confirms the self-limiting deposition mechanism, as once the compact surface hydroxide/oxyhydroxide layer is formed, the film thickness is no longer increasing with

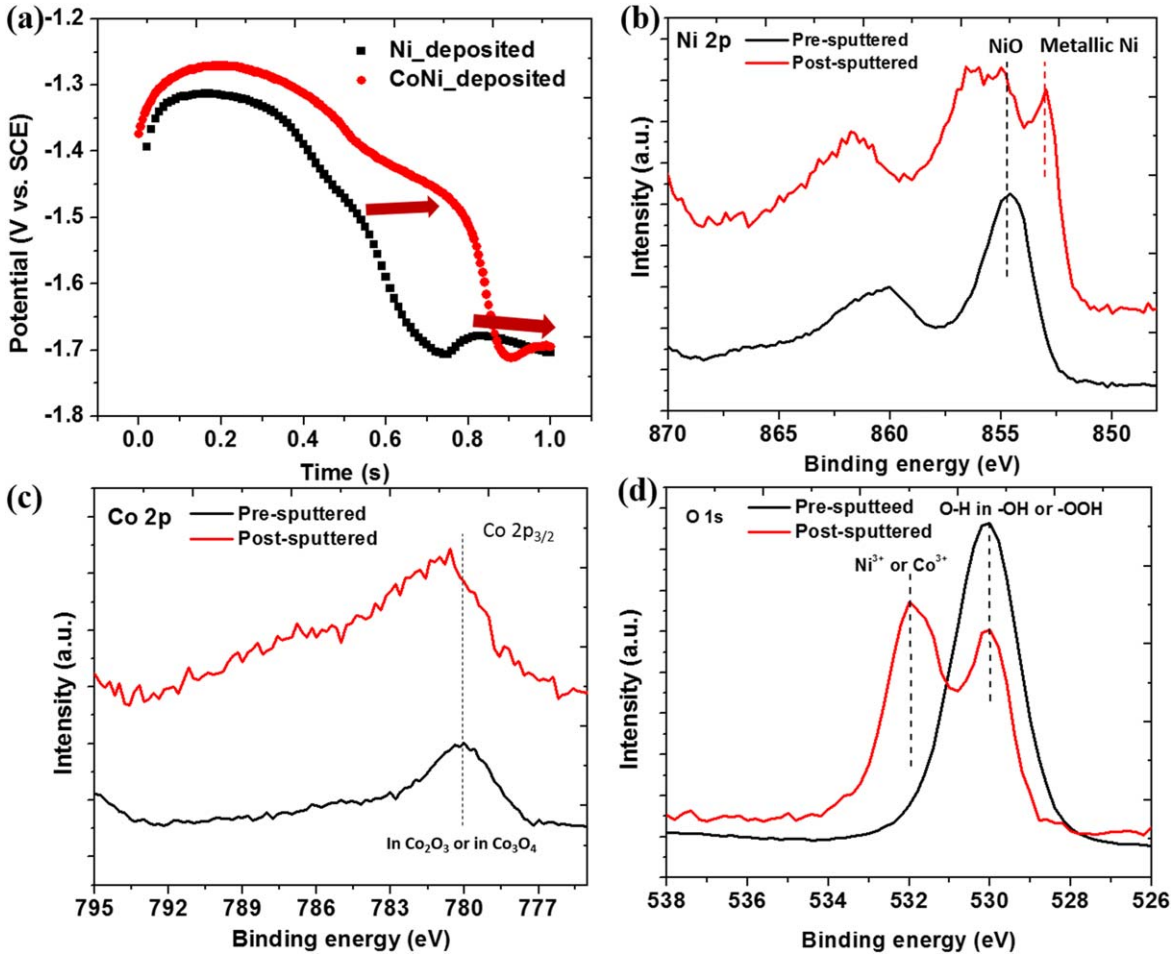

Figure 1. (a) Potential transients of Ni and Ni-Co on Au in the first second of galvanostatic electrodeposition. XPS spectrum of Ni (b), Co (c) and O (d) for Ni-Co film before/after 6 s Ar sputtering (Removed layer thickness is ~1.45 nm).

time. Oxygen composition for both films drops to zero at a depth of ~5 nm, implying a low thickness of the surface hydroxide/oxyhydroxide layer (⩽5 nm). The depth profile of Ni-Fe/Au was shown in Fig. 3b. Ni and Fe composition decreases after the first sputtering for both 10 s and 60 s deposition, as a result of the interdiffusion of Ni, Fe and Au. The composition variation when the Ar milling depth is less than 10 nm between the 10 s and 60 s deposited films is probably due to the anomalous electrodeposition between Ni and Fe,[14] in which case a slight change in the initial ratio of the Ni and Fe could result in a relatively larger difference in the products. However, the composition of Au along the depth for the 10 s Ni-Fe deposition overlaps with that for the 60 s Ni-Fe deposition while at ~20 nm the Au composition reaches ~100%. This indicates the Ni-Fe deposition is also independent of deposition time when the formation of surface hydroxide/oxyhydroxide layer is formed, and thus follows the self-limiting deposition mechanism. The grain size difference was further compared by GI-XRD as shown in Fig. 3d. The peak located at $2\theta = 44.5°$ corresponds the diffraction from Ni (111) plane. The full width at high maximum (FWHM) becomes broader for the Ni-Fe/GaAs, demonstrating that the grain size is finer for the Ni-Fe according to Scherrer equation. From the previous discussion, the self-limiting growth during deposition occurs in Ni, Ni-Co, and Ni-Fe deposition, while both the Ni-Co and Ni-Fe deposition have a slower nucleation process compared to Ni deposition.

Electrochemical/photoelectrochemical properties of Iron-group binary alloys.—The catalytic activity towards water oxidation for Co, Ni, Ni-Co and Ni-Fe were estimated by cyclic voltammetry measured in 1 M KOH as shown in Fig. 4a. The overpotential when the current density reaches 10 mA cm^{-2} is 0.644 V, 0.462 V, 0.428 V and 0.326 V for Ni, Co, Ni-Co and Ni-Fe film respectively as shown in Fig. 4b. The onset potential is significantly reduced at the surface of binary alloy films (Ni-Fe and Ni-Co) compared with pure metallic layer (Ni or Co). The Tafel plots were measured in the same condition to further estimate the electrochemical kinetics as shown in Fig. 4c, where a Tafel slope of 93 mV dec^{-1} and 49 mV dec^{-1} is obtained for Ni-Co and Ni-Fe film, while a Tafel slope of 137 mV dec^{-1} and 273 mV dec^{-1} is shown respectively for pure Ni and Co film. The reduced onset potentials and the smaller Tafel slopes of the alloy deposits indicate an enhanced OER kinetics comparing with the plain metals. The enhanced OER catalytic property is owed to an optimized bond strength between metal site and oxygen for NiOOH[15] as well as the additional active sites created by Fe or Co.[16]

Photoelectrochemical performance of Ni-Co/GaAs and Ni-Fe/GaAs was investigated in an aqueous solution containing $K_3Fe(CN)_6/K_4Fe(CN)_6$ under chopped light. Linear sweep voltammetries for the Ni-Co/GaAs and Ni-Fe/GaAs films were shown in Fig. 5a. Both of the films show similar onset potential of 0.5 V vs RHE corresponding to a photovoltage of ~0.39 V, while the saturated photocurrent density reaches 7.2 mA cm^{-2} at a ~1.0 V vs RHE in either case. The similar photoelectrochemical performance for Ni-Co/GaAs and Ni-Fe/GaAs is attributed to the fact that the self-limiting deposited Ni-Co and Ni-Fe has close thickness and the junction created on the interface has similar behavior. The only difference is the photocurrent density for Ni-Fe/GaAs before saturation is higher than that of Ni-Co/GaAs with a maximum value

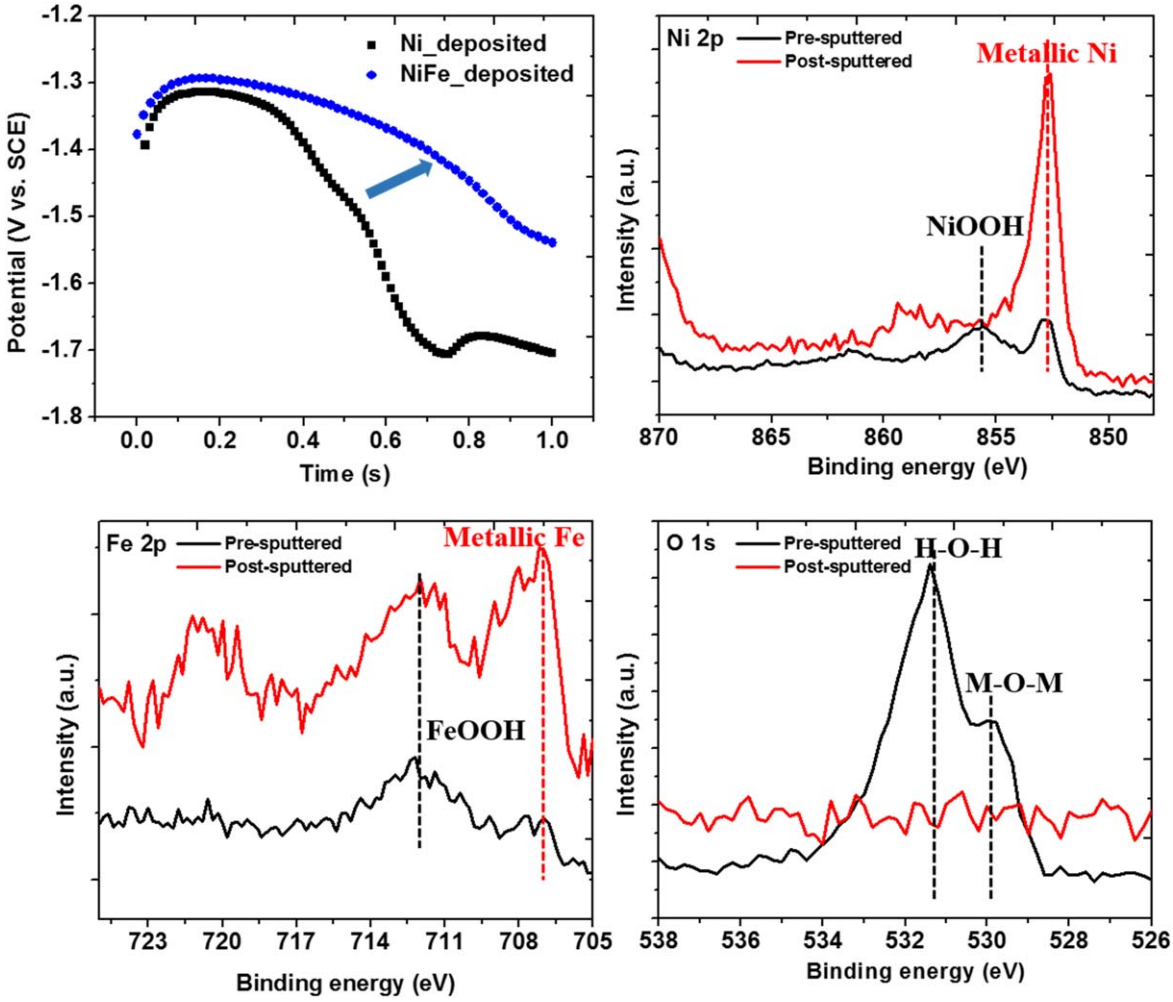

Figure 2. (a) Potential transients of Ni and Ni-Fe on Au in the first second of galvanostatic electrodeposition. XPS spectrum of Ni (b), Fe (c) and O (d) for Ni-Fe film before/after 6 s Ar sputtering.

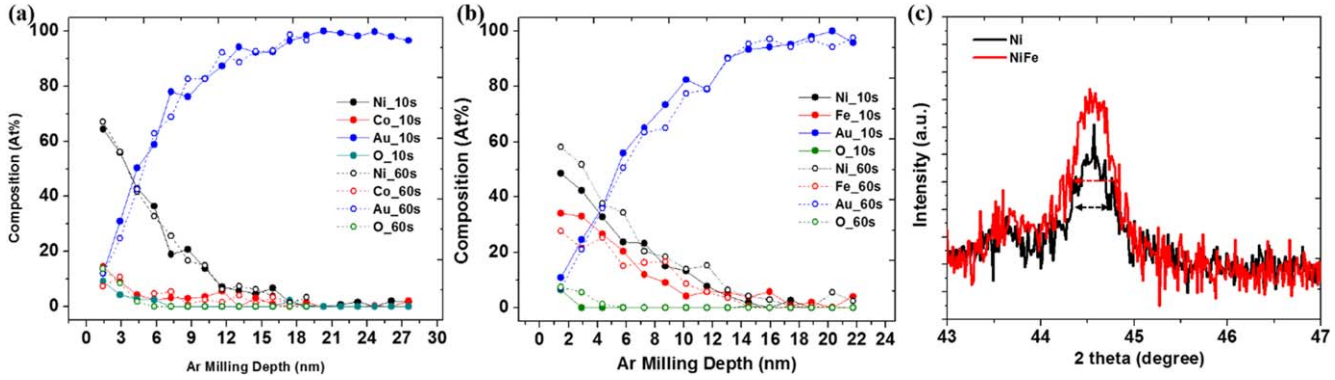

Figure 3. Elemental composition vs Ar milling depth for Ni-Co/Au (a) and Ni-Fe/Au (b) for 10 s (solid symbol) or 60 s (hollow symbol) deposition time. (c) GI-XRD for Ni and Ni-Fe film.

of 0.8 mA cm^{-2}, which is attributed to the superior electrochemical catalytic activity of Ni-Fe film as aforementioned leading to a more rapid oxidation kinetics on the surface of the photoanode. Figure 5b shows a comparison of stability between Ni/GaAs and Ni-Co/GaAs in the first 300 s potentialstatic measurements under the light at a potential of 1.23 V vs RHE with different deposition time of 0.2 s, 0.5 s and 1.0 s. For Ni/GaAs deposited for 0.2 s and 0.5 s, a rapid decay in photocurrent is shown in the first 30 s and a gradual decrease in photocurrent is present for the Ni/GaAs deposited for 1.0 s with a photocurrent retention of ~82.4%. For Ni-Co/GaAs deposited for 0.2 s, an obvious photocurrent decay exhibits after 200 s, while for 0.5 s and 1.0 s deposited Ni-Co/GaAs, photocurrent decrease is minimum with a retention of ~91.8%. The stability of Ni-Fe/GaAs in the first 300 s under the same condition is shown in Fig. 5c. 0.2s-deposited Ni-Fe exhibits a gradual decreased photocurrent in the first 300 s measurement, while no obvious photocurrent decay is present for 0.5 s and 1.0s-deposited Ni-Fe/GaAs and a maximum retention of 93.7% for 0.5 s deposited Ni-Fe/GaAs is

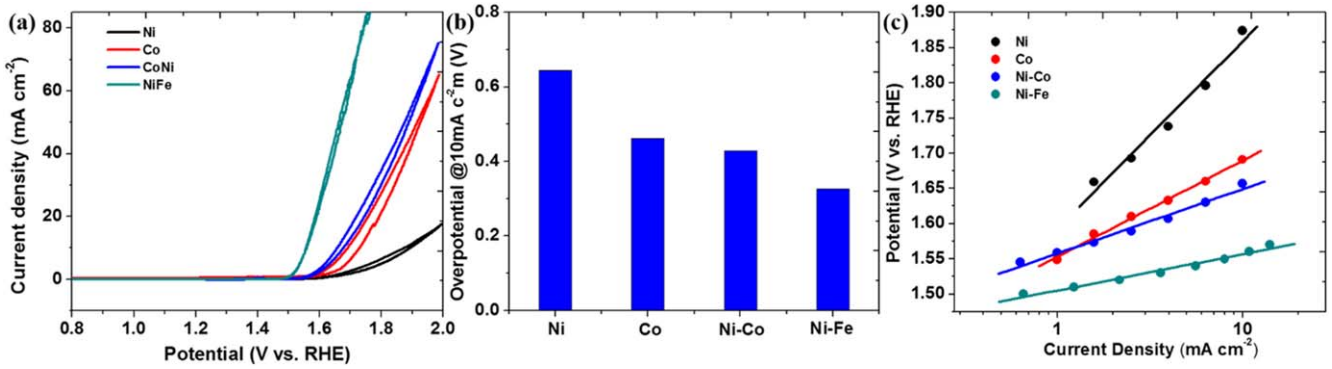

Figure 4. Cyclic voltammetries (a), overpotential at a current density of 10 mA cm^{-2} (b) and Tafel plots (c) for Ni, Co, self-limiting Ni-Co and self-limiting Ni-Fe films on Au in 1 M KOH.

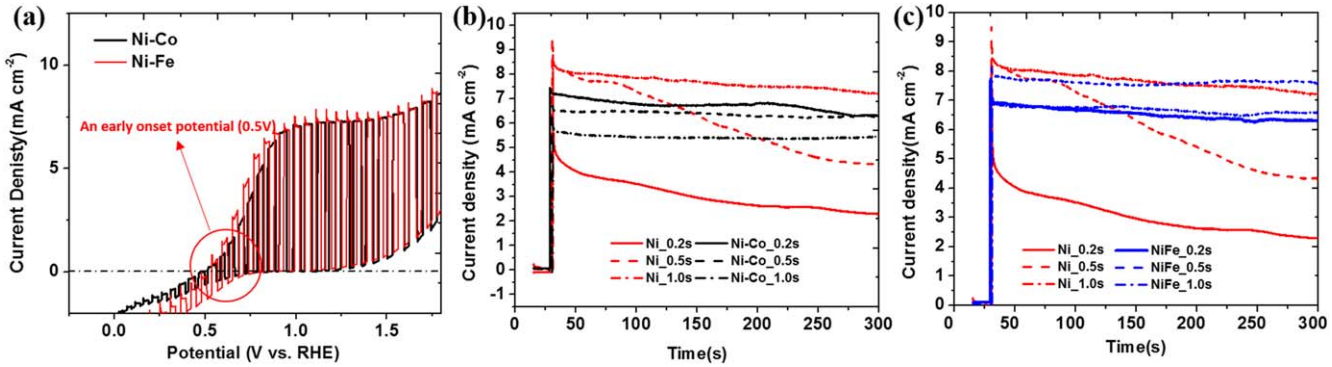

Figure 5. (a) Linear scanning voltammetries of self-limiting Ni-Co/GaAs and self-limiting Ni-Fe/GaAs samples under chopped irradiation of 100 mW cm^{-2} using AM 1.5 G solar simulator in a $K_3Fe(CN)_6/K_4Fe(CN)_6$ solution. (b) Photocurrent transient for Ni/GaAs and Ni-Co/GaAs in the first 300 s at 1.23 V vs RHE with various deposition time. (c) Photocurrent transient for Ni/GaAs and Ni-Fe/GaAs in the first 300 s at 1.23 V vs RHE with various deposition. Different colors indicate different samples, whereas different line styles indicate different deposition times.

shown. It need to be noted that the 0.5s-deposited Ni-Fe/GaAs still retains a high photocurrent density of 7.6 mA cm^{-2}. Ni-Co and Ni-Fe films exhibit improved stability towards photocorrosion compared to pure Ni film, attributed to a smaller particle size and thus a higher density of nanoislands on the surface. Ternary Iron-group film containing Ni, Co, and Fe is then investigated on Au or GaAs substrate, aiming at further improving the electrochemical/photoelectrochemical performance towards water oxidation.

Electrodeposition of iron-group trinary alloys on Au or GaAs.—XPS spectra for Ni-Co-Fe deposited on Au before/after 6s-Ar sputtering were collected for Ni, Co, Fe and O, and are shown in Figs. 6a–6d. Prior to Ar puttering, a peak from metallic Ni is found at a bonding energy of 852.8 eV while there are multiple peaks locating at 855–856 eV and 861–862 eV, possibly corresponding to Ni oxide/ (oxy) hydroxides. Theses peaks are hard to define with low intensity as the surface is highly oxidized in air and probably covered with absorbed water. After sputtering off a layer of ~1.5 nm, the spectrum shows a main peak locating at a binding energy of 852.8 eV and another peak with intense counts at 870 eV associated with Ni $2p_{3/2}$ and Ni $2p_{1/2}$ in metallic Ni while no other obvious peaks are shown. This implies that Ni mainly exists in the form of metal while no oxide/ (oxy) hydroxide is formed except on the surface, which further supports the self-limiting mechanism as the surface (oxy) hydroxides are not generated until the surface reaches coalescence. XPS spectrum of Co is shown in Fig. 6b, where no distinguishable peak is shown prior to sputtering due to the small amount of Co and the highly oxidized surface. A peak located at a binding energy of 778.3 eV is exhibited in the spectrum after sputtering, corresponding to metallic Co. No metallic Fe peak is shown on the surface before sputtering as can be seen in Fig. 6c, since Fe is also vulnerable to oxidation in air and the broad peak ranging from 711 eV to 713 eV can be probably assigned to FeOOH (711.3–711.8 eV). A metallic peak from Fe for the post-sputtered Ni-Fe-Co film is shown while the borad peak from FeOOH still exists, because of the diffusion of surface oxygen to Fe. Oxygen spectrum shown in Fig. 6d further confirms the fact that the surface of the pre-sputtered Ni-Fe-Co film is mainly covered with absorbed water molecules and oxides, as the peak occurring at 531.6 eV is close to H-O-H bond (532.0 to 532.4 eV) or M-O-H (531 to 532 eV) and the peak occurring at 530.0 eV is corresponding to M-O-M bond (529.6 to 531.8 eV from common Ni oxides, Co oxides and Fe oxides). The peak at 531.6 eV disappears while the intensity of the peak at 530.0 eV decreases significantly after Ar sputtering, indicating the film underneath the surface is mainly composed of metallic Ni, Co and Fe while there is still a small fraction of Fe oxyhydroxide due to the diffusion of oxygen.

XPS depth profile depicting the elemental composition change along the depth of the Ni-Co-Fe film for different deposition time is shown in Fig. 7. Ni composition starts to decrease after the first sputtering and stays less than 5 At% when the milling depth is more than 18 nm as shown in Fig. 7a. The relative large thickness in the interface between Ni and Au is attributed to the interdiffusion similar to Ni-Co deposition. The composition profile of 10s-deposited and 60 s deposited sample overlaps despite negligible deviations, indicating the independence of the film thickness towards deposition time. Figure 7b exhibits the Fe composition profile for the 10 s and 60 s deposited Ni-Fe-Co film. A plateau occurs for a depth of less than ~8 nm, and the composition starts to decrease as the interdiffusion between Fe and Au occurs. For Co depth profile shown in Fig. 7c, a decrease in the film does not occur until the milling depth is larger than ~10 nm. The deviation between 10 s and 60 s

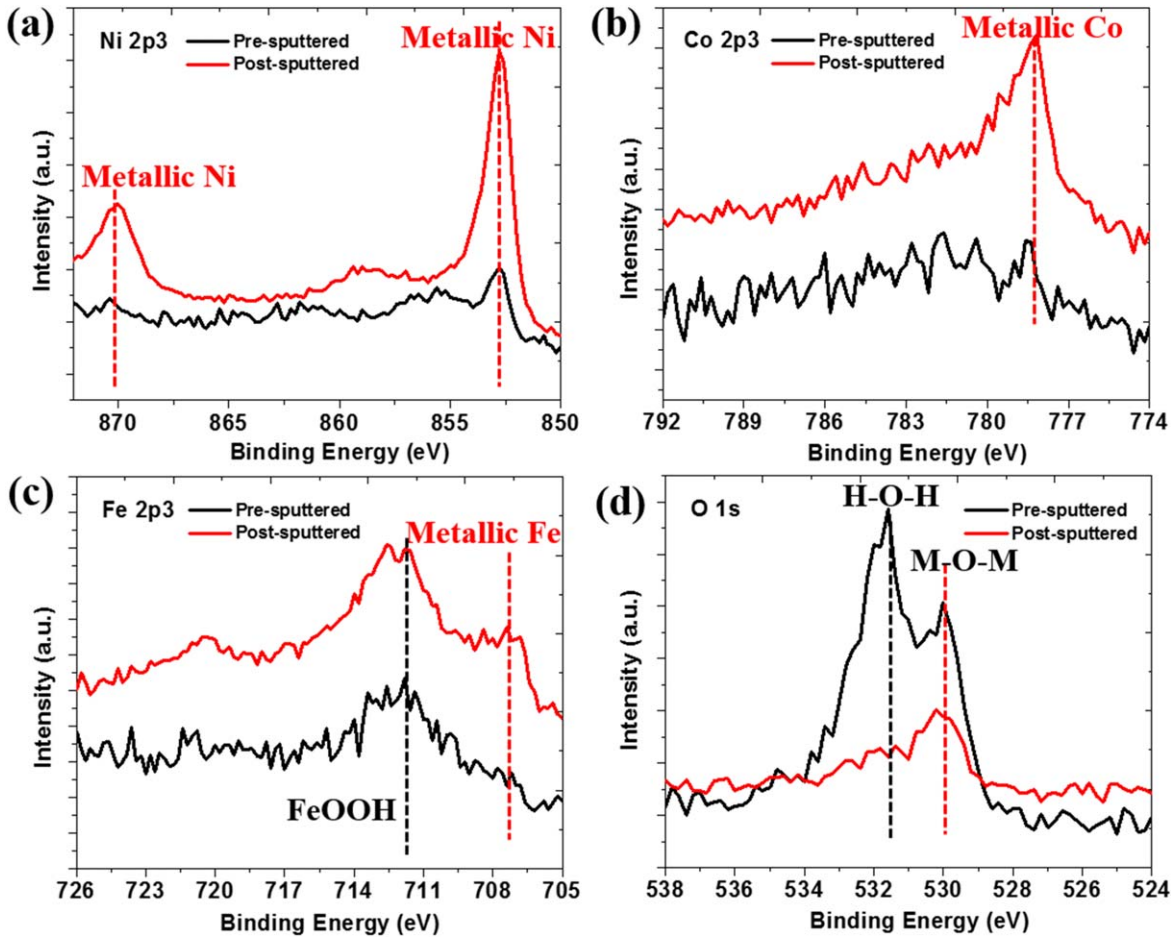

Figure 6. XPS spectrum of Ni (a), Co (b), Fe (c) and O (d) for the Ni-Fe-Co films on Au.

deposited film is relatively large due to the relatively small amount of Co (∼10 At%) in the film. Au depth profile for the 10 s and 60 s deposited film is shown in Fig. 7d, the increase in composition with depth is owed to the interdiffusion while the similarity between 10 s and 60 s deposited films further verifies that the film thickness is independent of deposition time. Oxygen composition is dropping to zero at ∼5 nm depth for both films with different deposition time, which implies the thickness of surface oxide/(oxy)hydroxide layer is ∼5 nm. Potential transient vs deposition time in the first 3 s for the Ni-Fe-Co deposition is shown in Fig. 7f. A potential bump featuring the formation of hydroxide layer occurs at 1.5 s as marked out, which is later than Ni (∼0.6 s), Ni-Co (∼0.8 s), and Ni-Fe (∼0.8 s) deposition, as a result of a slower nucleation process by adding a third element.

Electrochemical/photoelectrochemical properties of the Iron-group trinary alloys.—In order to investigate the electrochemical performance of the trinary alloys films. Linear scanning voltammetries for various deposition time (1 s to 60 s) measured in 1 M KOH is shown in Fig. 8a. The oscillation of the curves at higher potential (⩾1.6 V) is owed to the intense hydrogen bubble formation on the surface. The overpotential at 10 mA cm^{-2} for the Ni-Fe-Co film is 0.314 V, 0.319 V, 0.316 V and 0.32 V for a deposition time of 1 s, 10 s, 30 s and 60 s, respectively, as shown in Fig. 8b. Tafel measurements in 1 M KOH was applied to study the electrochemical kinetics of water oxidation on the surface of Ni-Fe-Co film and Tafel plots are shown in Fig. 8c. For all the films with different deposition time, the overpotential follows a good linear relationship with the logarithm of current density, verifying water oxidation is the main reaction in the selected potential range. A Tafel slope of 34.7, 37.9 and 38.4 mV dec^{-1} is respectively exhibited for 1 s, 10 s and 60 s deposited films, showing a much enhanced electrochemical kinetics compared to Ni-Fe (49 mV dec^{-1}), Ni-Co (93 mV dec^{-1}) and Ni (273 mV dec^{-1}). The slightly improved property of 1 s deposited Ni-Fe-Co film compared to 10 s deposited film is probably due to an increased resistance in the film with increased thickness as for a deposition time of 1 s, the surface compact (oxy) hydroxide layer is not formed and the film thickness is still dependent of the deposition time. For a longer deposition time of 60 s, both the onset potential and the Tafel slope slightly increase as more pinholes are generated on the surface caused by the intense hydrogen evolution during the deposition.

The photoelectrochemical performance of the Ni-Fe-Co deposited on GaAs with different deposition time is investigated in an aqueous Ferri/Ferro cyanide solution under AM 1.5 G solar illumination with a power density of 100 mW cm^{-2}. Linear scanning voltammetries are shown in Fig. 9a. The saturated photocurrent density for all the three films are similar with a value of ∼4.7 mA cm^{-2}. For the 1s-depostied Ni-Fe-Co/GaAs, an onset potential of 0.58 V vs RHE is obtained corresponding to a photovoltage of 0.29 V, while the onset potential is 0.70 V for both 10 s and 30 s deposited film as shown in Fig. 9b. The similar photoresponse for 10 s and 30 s deposited film is owed to the close thickness and composition of the Ni-Fe-Co film when the self-limiting condition is fulfilled, while the Fermi level pinning effect when coalescence is reached leads to a late onset potential.[17] The stability of Ni-Fe-Co deposited GaAs is investigated by potentiostatic measurement at 1.23 V vs RHE under the light and is compared with the previous results obtained on Ni/GaAs, Ni-Co/GaAs, Ni-Fe/GaAs. The optimal photocurrent retention of the different alloy-systems is shown in Fig. 9c, where Ni-Fe-Co/GaAs

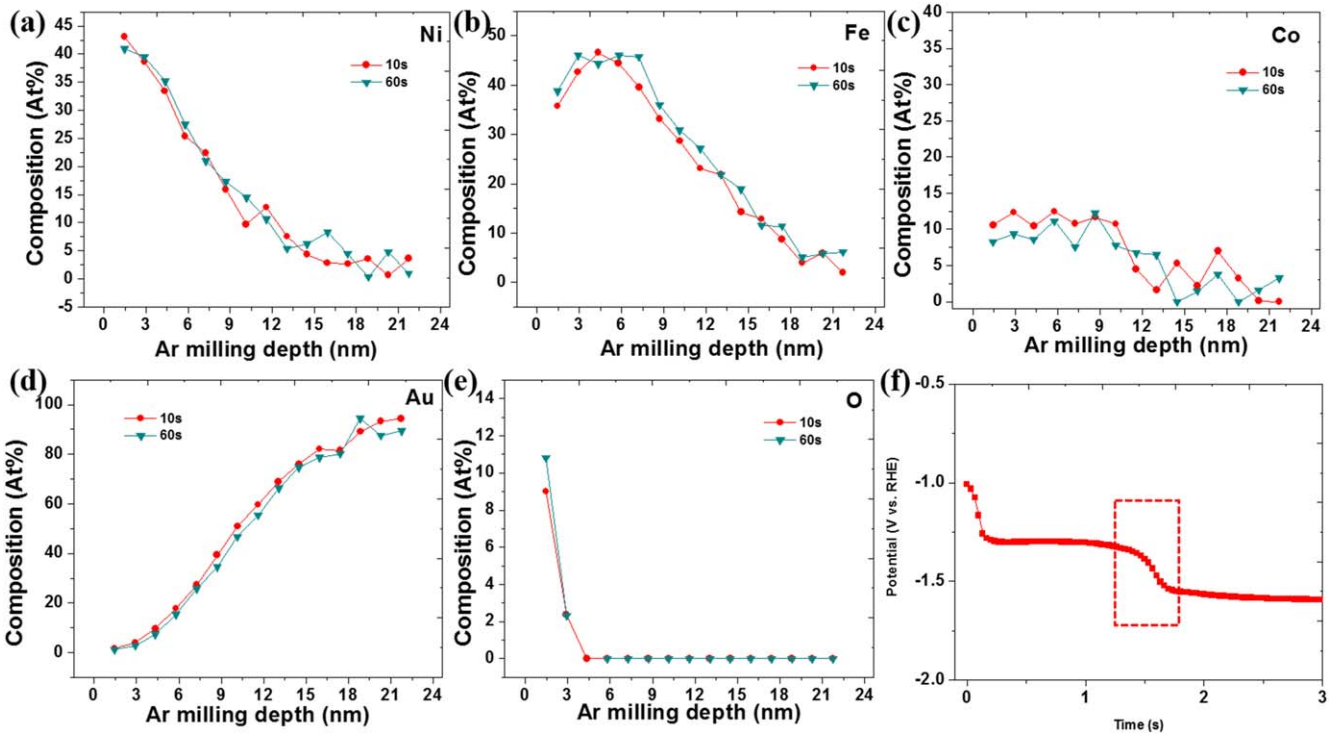

Figure 7. Elemental composition vs Ar milling depth for Ni (a), Fe (b), Co (c), Au (d), and O (e) for Ni-Fe-Co/Au. The element of the figure is labeled at the top-right corner, different colors mean different deposition times. (f) Potential transient of Ni-Fe-Co deposition on Au in the first 3 s with current density 10 mA cm^{-2}.

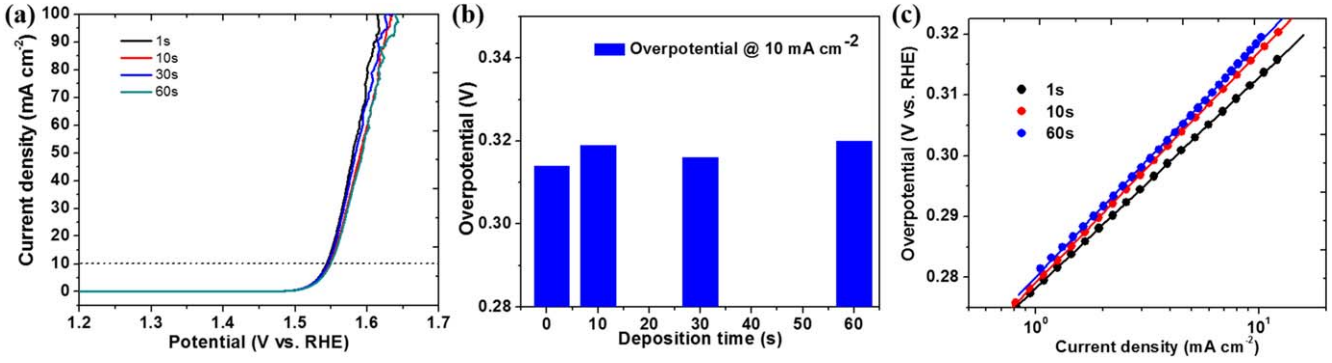

Figure 8. linear scanning voltammetries (a), overpotential at a current density of 10 mA cm^{-2} (b) and Tafel plots (c) for Ni-Fe-Co with deposition time ranging from 1 s to 60 s. Different colors indicate different deposition times.

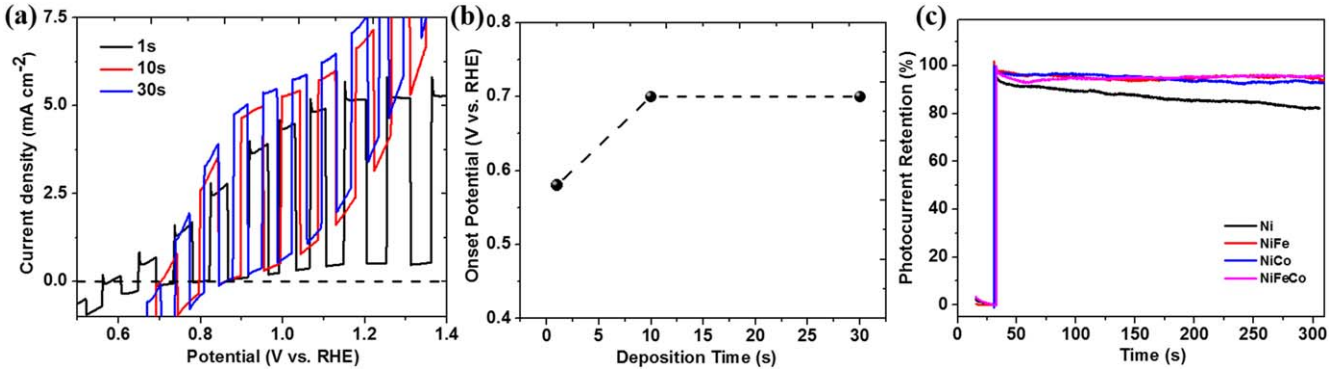

Figure 9. (a) Linear scanning voltammetries of Ni-Fe-Co/GaAs deposited with different time under chopped irradiation of 100 mW cm^{-2} using AM 1.5 G solar simulator in a $K_3Fe(CN)_6/K_4Fe(CN)_6$ solution. Different colors indicate different times. (b) Onset potential of Ni-Fe-Co/GaAs deposited at various deposition time. (c) Comparison of photocurrent retention of Ni, Ni-Fe, Ni-Co and Ni-Fe-Co/GaAs in a 300 s potentialstatic measurement under light. Different colors indicate different compositions of the deposits.

exhibits the optimum photocurrent retention (96.36%) compared to the binary alloy films or Ni film deposited on GaAs.

Conclusions

In this work, the self-limiting electrodeposition of two binary Iron-group mutual alloy films (Ni-Co and Ni-Fe) and one ternary Iron-group mutual alloy film (Ni-Co-Fe) are investigated. The self-limiting mechanism is substantiated by potential transient during deposition, XPS spectrum and XPS depth profile, as the formation of (oxy) hydroxide/metal layer with low thickness, high coalescence is independent on deposition time. We also demonstrate that by adding an external element leads to a slower nucleation process due to a smaller grain size of the deposited nanoislands as indicated by GI-XRD. The various Iron-group mutual alloy films deposited on Au substrate were further investigated as electrochemical catalysts for water oxidation in 1 M KOH. Both binary and ternary Iron-group mutual alloy films exhibit improved water oxidation kinetics compared to pure Ni or Co film. In particular, an overpotential of 0.314 V at 10 mA cm^{-2} and a Tafel slope of 34.7 mV dec^{-1} are obtained on the Ni-Fe-Co film. In addition, the Iron-group mutual alloys deposited on GaAs were further investigated as photoanodes in an aqueous Ferri/Ferrocyanide solution under the light. The binary mutual alloy films exhibit high photocurrent density (7.2 mA cm^{-2}) with low onset potential (0.5 V vs RHE) and an improved stability compared to pure Ni film, while the stability towards photocorrosion can be further improved by using the trinary mutual alloy films with the cost of a reduced photoresponse (4.7 mA cm^{-2}). This work provides a new deposition scheme to access continuous ultrathin Iron-group alloys with various composition, while to tailor the Ni-Fe-Co composition in the trinary alloy system is possible to further improve the electrochemical/photoelectrochemical performance.

Acknowledgments

We acknowledge financial support from the University of Virginia through the MAXNET Energy partnership.

ORCID

Yunkai Sun https://orcid.org/0000-0001-8044-4936
Massimo Innocenti https://orcid.org/0000-0002-4179-0032

References

1. A. Kudo and Y. Miseki, "Heterogeneous photocatalyst materials for water splitting." *Chem. Soc. Rev.*, **38**, 253 (2009).
2. J. D. Holladay, J. Hu, D. L. King, and Y. Wang, "An overview of hydrogen production technologies." *Catal. Today*, **139**, 244 (2009).
3. M. G. Walter, E. L. Warren, J. R. McKone, S. W. Boettcher, Q. Mi, E. A. Santori, and N. S. Lewis, "Solar water splitting cells." *Chem. Rev. (Washington, DC, United States)*, **110**, 6446 (2010).
4. Y. Xu, R. Ahmed, Q. Lin, and G. Zangari, "(Photo) electrochemical water oxidation at anodic TiO2 nanotubes modified by electrodeposited NiFe oxy-hydroxides catalysts." *Electrochim. Acta*, **308**, 91 (2019).
5. M. Gong and H. Dai, "A mini review of NiFe-based materials as highly active oxygen evolution reaction electrocatalysts." *Nano Res.*, **8**, 23 (2015).
6. I. Roger, M. A. Shipman, and M. D. Symes, "Earth-abundant catalysts for electrochemical and photoelectrochemical water splitting." *Nat. Rev. Chem.*, **1**, 3 (2017).
7. S. Hu, M. R. Shaner, J. A. Beardslee, M. Lichterman, B. S. Brunschwig, and N. S. Lewis, "Amorphous TiO2 coatings stabilize Si, GaAs, and GaP photoanodes for efficient water oxidation." *Science*, **344**, 1005 (2014).
8. W. Giurlani, G. Zangari, F. Gambinossi, M. Passaponti, E. Salvietti, F. Di Benedetto, S. Caporali, and M. Innocenti, "Electroplating for decorative applications: recent trends in research and development." *Coatings.*, **8**, 260 (2018).
9. J. Vanpaemel, M. H. van der Veen, S. De Gendt, and P. M. Vereecken, "Enhanced nucleation of Ni nanoparticles on TiN through H3BO3-mediated growth inhibition." *Electrochim. Acta*, **109**, 411 (2013).
10. J. Vanpaemel, M. Sugiura, D. Cuypers, M. H. Van Der Veen, S. De Gendt, and P. M. Vereecken, "Electrochemical deposition of subnanometer Ni films on TiN." *Langmuir*, **30**, 2047 (2014).
11. N. L. Ritzert and T. P. Moffat, "Ultramicroelectrode studies of self-terminated nickel electrodeposition and nickel hydroxide formation upon water reduction." *, J. Phys. Chem. C.*, **120**, 27478 (2016).
12. R. Wang, U. Bertocci, H. Tan, L. A. Bendersky, and T. P. Moffat, "Self-terminated electrodeposition of Ni, Co, and Fe ultrathin films." *J. Phys. Chem. C*, **120**, 16228 (2016).
13. C. Scheck, P. Evans, G. Zangari, and R. Schad, "Sharp ferromagnet/semiconductor interfaces by electrodeposition of Ni thin films onto n-GaAs (001) substrates." *Appl. Phys. Lett.*, **82**, 2853 (2003).
14. D. Gangasingh and J. B. Talbot, "Anomalous electrodeposition of nickel-iron." *J. Electrochem. Soc.*, **138**, 3605 (1991).
15. R. Subbaraman, D. Tripkovic, K.-C. Chang, D. Strmcnik, A. P. Paulikas, P. Hirunsit, M. Chan, J. Greeley, V. Stamenkovic, and N. M. Markovic, "Trends in activity for the water electrolyser reactions on 3d M (Ni, Co, Fe, Mn) hydr (oxy) oxide catalysts." *Nat. Mater.*, **11**, 550 (2012).
16. D. Friebel, M. W. Louie, M. Bajdich, K. E. Sanwald, Y. Cai, A. M. Wise, M.-J. Cheng, D. Sokaras, T.-C. Weng, and R. Alonso-Mori, "Identification of highly active Fe sites in (Ni, Fe) OOH for electrocatalytic water splitting." *J. Am. Chem. Soc.*, **137**, 1305 (2015).
17. J. C. Hill, A. T. Landers, and J. A. Switzer, "An electrodeposited inhomogeneous metal-insulator-semiconductor junction for efficient photoelectrochemical water oxidation." *Nat. Mater*, **14**, 1150 (2015).